International Immunopharmacology 153 (2025) 114489

Contents lists available at ScienceDirect

International Immunopharmacology

journal homepage: www.elsevier.com/locate/intimp

Doxorubicin promotes NK cell dysfunction and induces acute liver injury through kynurenine-AhR axis

Bohuai Tang [a,1], Huan Ouyang [b,1], Shuping Zheng [c,1], Le Yu [a], Ruiying Xiao [a], Linqing Wu [a,*], Zengbin Wang [a,*]

[a] Department of Immunology, School of Basic Medical Sciences, Fujian Medical University, Fuzhou, 350122, China
[b] Department of Cardiovascular, The First Affiliated Hospital, Fujian Medical University, Fuzhou, Fujian, 350004, China
[c] Public Technology Service Center, Fujian Medical University, Fuzhou, 350122, China

ARTICLE INFO

Editor: Yi-Chao Zheng

Keywords:
Doxorubicin
DILI
L-kynurenine
NK cell
IDO2

ABSTRACT

Drug-induced liver injury (DILI) is one of the significant drug-induced diseases and a major cause of clinically unexplained liver injury and unexplained liver diseases. However, the mechanisms underlying doxorubicin (DOX)-induced DILI remain unclear. In this study, we constructed a mouse model of DOX-induced acute liver injury (ALI) and employed a combination of proteomics, metabolomics, and flow cytometry (FCM) to examine the roles of metabolic processes and innate immune responses. Our findings revealed that DOX treatment altered the metabolic profile and innate immune response signals in mouse livers. Specifically, DOX activated the indoleamine 2,3-dioxygenase 2 (IDO2)-mediated L-Tryptophan/L-Kynurenine metabolic pathway. Further in-depth analysis demonstrated that DOX promoted natural killer (NK) cell dysfunction leading to ALI by activating the kynurenine-aryl hydrocarbon receptor (Kyn-AhR) axis. Importantly, targeting the Kyn-AhR axis could reverse DOX-induced ALI. In summary, this study suggests that targeting the Kyn-AhR axis holds promise as an effective strategy to reverse ALI.

1. Introduction

The annual incidence of drug-induced liver injury (DILI) in the general Chinese population is 23.80 per 100,000 individuals. Among these cases, more than half are hepatocyte-injury type, 28.3 % are mixed type, and 20.31 % are cholestatic type [1]. Studies showed that DILI has now become the second most common reason for liver biopsy after chronic hepatitis B. The Council for International Organizations of Medical Sciences (CIOMS) DILI Working Group released the "International Consensus on Drug-Induced Liver Injury" in 2020. Currently, not only Doxorubicin (DOX), but also many traditional Chinese medicines such as dysosma versipellis (DV) can cause liver damage or cardiac toxicity [2–4]. However, the relationship between other drugs including *Houttuynia cordata* Thunb. [5], R. rubescent [6] and LJP [7] and liver injury is not yet clear. Our previous research found that treatment with recombinant interleukin-33 (IL-33) can alleviate acetaminophen (APAP)-induced DILI in mice [8]. However, there are numerous unmet clinical needs regarding the pathogenesis, risk factors, clinical diagnosis, and effective interventions for DILI.

DOX is a broad-spectrum anticancer drug used to treat various malignancies, including liver cancer, breast cancer, ovarian cancer, leukemia, and lymphoma [9]. Transarterial chemoembolization or systemic DOX chemotherapy is the preferred treatment for unresectable hepatocellular carcinoma (HCC). The most common side effects of DOX are hematopoietic failure, cardiotoxicity, and liver injury. Approximately 40 % of patients receiving DOX experience liver damage [10]. Studies indicated that DOX induces cardiac dysfunction by increasing levels of oxidative stress products, apoptotic factors, proinflammatory cytokines, and autophagy markers, leading to the triggering of cardiomyopathy and congestive heart failure [11,12]. Inhibiting oxidative stress and ER-mediated apoptosis can alleviate DOX-induced cardiotoxicity [13]. The mechanisms of DILI include mitochondrial dysfunction, lysosomal damage, the generation of endoplasmic reticulum (ER) stress, and the involvement of the immune system. After cellular stress, the accumulation of large amounts of DNA can trigger different DNA sensors, including cyclic GMP-AMP synthase (cGAS) and stimulator of interferon

* Corresponding authors.
E-mail addresses: wulinqing@fjmu.edu.cn (L. Wu), wangzengbin@fjmu.edu.cn (Z. Wang).
[1] These authors contributed equally to this work.

https://doi.org/10.1016/j.intimp.2025.114489
Received 19 February 2025; Received in revised form 4 March 2025; Accepted 12 March 2025
Available online 19 March 2025

genes (STING), leading to STING-mediated interferon regulatory factor 3 (IRF3) activation and the production of type I interferons [14]. Our previous research demonstrated that cGAS and STING signaling are activated during DILI [15]. However, the production of inflammatory factors, the activation of inflammatory signaling pathways, and the regulatory mechanisms of immune cells during DOX-induced DILI remain unclear.

In this study, we explored the roles of metabolism and innate immune response in DOX induced acute liver ALI in mice using proteomics, metabolomics, and flow cytometry (FCM). This study focuses on elucidating the mechanism of IDO2 mediated Kyn-AhR axis regulation of NK cell dysfunction leading to ALI, providing a solid experimental basis for further development of liver protection strategies.

2. Materials and methods

2.1. Reagents

The following reagents were sourced from their respective manufacturers: Dulbecco's Modified Eagle Medium (Grand Island, NY); penicillin-streptomycin (Solarbio, Beijing, China); Phosphate-buffered saline (PBS) (Solarbio, Beijing); Type IV Collagenase (Collagenase IV) (Sigma-Aldrich, CAS C5138); Cell Staining Buffer (Biolegend, CAS 420201); Deoxyribonuclease I (Sigma-Aldrich, CAS DN25); Doxorubicin (Dox) (Shanghai yuanye Bio-Technology Co., Ltd., CAS 25316–40-9); Hematoxylin-Eosin (HE) Stain Kit (Solarbio, CAS G1120); IDO2-IN-1 (HY-151093, MedChemExpress LLC); L-Kynurenine (L-Kyn) (HY-104026, MedChemExpress LLC); CH-223191 (HY-12684, MedChemExpress LLC).

2.2. Animal model assay

For the animal model assay, male C57BL/6 N mice, aged six to eight weeks and weighing approximately 17–21 g, were obtained from Shanghai SLAC Laboratory Animal Co., Ltd. These animals were housed in a specific pathogen-free (SPF) environment, where the temperature was maintained at 21–23 °C and the humidity was controlled at 40–55 % to ensure optimal conditions for their well-being. Mice were fed with SPF grade sterile nutritional granules. The animal experiments were carried out according to the Institutional Animal Care and Use Committee guidelines and were approved by the Experimental Animal Ethics Committee of Fujian Medical University (IACUC FJMU 2024–0035).

2.3. Dox induced mouse liver injury model

C57BL/6 N mice were randomly divided into a control group (Ctrl) and an experimental group (DOX), with 8 mice in each group. The DOX group injected mice intraperitoneally with DOX (5 mg/kg, dissolved in PBS) every 2 days, for a total of 4 injections [16]. The subordinates of the Ctrl group were injected with the same volume of PBS. We measured the weight of mice every 2 days. On the seventh day, euthanasia was performed by administering anesthesia to the mice. Mouse liver tissue and blood were extracted for subsequent research. For the treatment of IDO2-IN-1, considering timeliness and comparability, we administered IDO2-IN-1 (25 mg/kg) intraperitoneally [17] on the 5th day of DOX treatment. For the treatment of AhR inhibitor (CH-223191, CH), we used intraperitoneal injection of CH (10 mg/kg) once a day for three consecutive days. Six mice were randomly selected for each treatment group. If the weight of the mice decreased by 20 % of their pre-experiment weight, we immediately provided end-of-life care by anesthetizing the mice and euthanizing them with cervical dislocation.

2.4. Hematoxylin-Eosin (HE) staining

Mouse liver tissue was collected. We washed the liver tissue with PBS, then fixed it with paraformaldehyde and embedded it in paraffin, and sliced it. According to the manufacturer's instructions, the sections were stained and examined under an optical microscope for histopathological analysis. We calculate the percentages of ballooning degeneration and necrotic liver cells separately.

Mouse serum analyses.

Serum was separated by centrifugation at 4000 rpm for 10 min. The serum alanine aminotransferase (ALT), aspartate aminotransferase (AST) and GSH levels were determined using an assay kit (Jiancheng Bioengineering Institute, Nanjing, China) according to the manufacturer's instructions. Serum TNF-α, IL-1β, IL-6 and IL-10 levels were measured using commercially available enzyme-linked immunosorbent assay (ELISA) kits (Elabsceience Bio) following the manufacturer's instructions.

2.5. Cell lines and cell culture, treatment and transfection

HepaRG cells were obtained from Shanghai Guandao Biological Engineering Co., Ltd., maintained in RPMI 1640. NK-92 cells were acquired commercially from Procell Life Science & Technology Co., Ltd. The culture medium employed for culturing NK-92 cells consists of MEMα supplemented with 0.2 mM inositol, 0.1 mM β-mercaptoethanol, 0.02 mM folic acid, 200 U/mL of recombinant interleukin-2 (IL-2) and 12.5 % horse serum. All cells were supplemented with 10 % FBS and 100 U/mL Penicillin/Streptomycin at 37 °C in a 5 % CO_2 atmosphere. To create stable HepaRG/shIOD2 cells, the cells were transfected with shIOD2 plasmids (GenaPharma, Shanghai, China) using lipofectamine 3000 and selected by puromycin upon standard protocols.

For the treatment of NK-92 cells. We filtered the culture medium of HepaRG/R cells cultured for 36 h, and used the filtered medium to treat NK-92 cells for 24 h with or without CH-223191 (5 μM) pretreatment for 1 h.

2.6. Construction of DOX resistant liver cells

The DOX-resistant liver cells, designated as HepaRG/R, were derived from the parental normal liver cells, HepaRG, through a gradual selection process involving increasing concentrations of DOX (ranging from 0.1 to 10 μg/mL) to induce resistance. These resistant cells were subsequently maintained in a culture medium containing 5 μg/mL of DOX.

2.7. Measurement of L-Kyn concentration

The concentration of L-Kyn (L-kynurenine) in the culture supernatant was then determined utilizing the Kynurenine ELISA Kit sourced from Abcam, with all procedures conducted strictly in accordance with the manufacturer's instructions.

2.8. Quantitative reverse transcription-polymerase chain reaction (qRT-PCR)

Total RNA was extracted using Trizol reagent (Thermo Fisher, Waltham, MA) following the manufacturer's instructions. Subsequently, 2 micrograms of total RNA were reverse-transcribed into cDNA using the Revert Aid First Strand cDNA Synthesis Kit (Thermo Fisher). Quantitative reverse transcription-polymerase chain reaction (qRT-PCR) was carried out on a QuantStudio 3 instrument (Thermo Fisher) with Fast Start Universal SYBR Green Mix (Roche, Mannheim, Germany). The primers were synthesized by Sangon Biotech (Shanghai, China). The relative mRNA levels were calculated using the $2^{-\Delta\Delta Ct}$ method, and the fold changes in gene expression were determined relative to the control. GAPDH served as the internal control for normalization.

The primer sequence is as follows: AhR, F: 5′-ACATCACCTACGCCAGTCG-3′, R: 5′-CGCTTGGAAGGATTTGACTTGA-3′; CD107a, F: 5′-CACGAGAAATGCAACACGTTAC-3′, R: 5′-GGGTGCCACTAACACATCTGTAT-3′; IFN-γ, F: 5′-TCGGTAACTGACTTGAATGTCCA-3′, R: 5′-TCGCTTCCCTGTTTTAGCTGC-3′.

2.9. 4D label-free quantitative proteomic analysis

4D-DIA quantitative proteomics was performed and analyzed by Panomix Biomedical Tech Co., Ltd. (Suzhou, China). The main steps included: protein extraction, digestion and cleanup, LC–MS/MS analysis, database search and quantification.

2.10. Whole target metabolomics sequencing

Whole target metabolomics sequencing was performed and analyzed by Panomix Biomedical Tech Co., Ltd. (Suzhou, China). The specific steps are as follows: (1) Data preprocessing: the raw data underwent conversion to mzXML format using MSConvert, a component of the ProteoWizard software package (version 3.0.8789). Subsequently, the data was processed with R XCMS (version 3.12.0) for feature detection, retention time correction, and alignment; (2) Metabolite identification: the metabolites were identified by matching their accurate mass and MS/MS data with various databases, including HMDB (http://www.hmdb.ca), MassBank (http://www.massbank.jp/) and KEGG (https://www.genome.jp/kegg/). The molecular weight of the metabolites was determined based on the *m/z* (mass-to-charge ratio) of parent ions in the MS data. The molecular formula was predicted using ppm (parts per million) and adduct ion information, and then matched with the database; (3) Data analysis: To discriminate between groups, two distinct multivariate statistical analysis models—unsupervised and supervised—were employed using the R ropls package (version 1.22.0). These models included PCA, PLS-DA, and OPLS-DA. The statistical significance of the *P*-value was determined through statistical testing between groups. To screen for biomarker metabolites, a combination of *P*-value, VIP (OPLS-DA variable projection importance), and FC (fold change between groups) was used. By default, metabolites with a *P*-value <0.05 and VIP value >1 were considered to have significant differential expression; (4) Pathway analysis: the differential metabolites were subjected to pathway analysis using MetaboAnalyst, which integrates powerful pathway enrichment analysis with pathway topology analysis. The identified metabolites from the metabolomics study were mapped to the KEGG pathway for biological interpretation of higher-level systemic functions.

2.11. Correlation analysis between metabolomics and proteomics

The correlation analysis between metabolomics and proteomics was conducted utilizing the two-way orthogonal partial least squares (O2PLS) method. O2PLS serves as an unsupervised modeling technique capable of objectively depicting the presence of a correlation trend between two datasets. To perform the O2PLS analysis, OmicsPLS in the *R* language was employed. All differential metabolites and proteins were selected to establish the O2PLS model. Subsequently, load graphs were utilized to preliminary identify variables with high correlation and weight. This step facilitated the screening of critical variables that exert a significant influence on the other omics dataset.

2.12. Immunoblotting

Cells were lysed using RIPA buffer containing protease inhibitors and PMSF for a duration of 15 min at 4 °C. Protein concentrations were accurately measured using a BCA assay to ensure consistent loading in subsequent steps. The protein complexes were resolved on SDS-PAGE gels, which were then used to transfer the proteins onto PVDF membranes. To prevent non-specific binding, the membranes were blocked with 5 % skim milk for 1 h at room temperature. Immunoblotting was performed using specific primary antibodies at a dilution of 1:1000 overnight at 4 °C. The primary antibodies used were as follows: IDO2 (Proteintech, CAS 30530–1-AP, 1:1000) and GAPDH (Cell Signaling Technology, CAS 2118, 1:1000). Following the overnight incubation, the membranes were washed and incubated with HRP-conjugated secondary antibodies for 1 h at room temperature. Bands were detected using a hypersensitive ECL kit, allowing for clear visualization and quantification of the target proteins.

2.13. Flow Cytometry (FCM)

Liver tissue samples were meticulously washed with PBS to remove any contaminants. The tissue was then minced into small pieces, approximately 3 to 5 mm in diameter, using scalpels. Digestion was performed using a mixture of 1 mg/mL collagenase IV, 10 mg/mL DNase I, 10 % FBS, and RPMI 1640 at 37 °C for 45 min, utilizing the gentle MACS Octo Dissociator with Heaters and continuous shaking to ensure thorough digestion. Following digestion, the homogenate was filtered through a 70 μm cell strainer to remove any larger debris or undigested tissue fragments. The filtered homogenate was then centrifuged at 400 $\times g$ for 8 min at 4 °C to sediment the cells. The cell suspension was carefully layered on top of 5 mL of Ficoll Plus separation buffer (#P4350, Solarbio, Beijing) and centrifuged at 900 $\times g$ for 30 min to clearly separate the cellular layers. After centrifugation, the single-cell suspension was washed in PBS and centrifuged once again at 400 $\times g$ for 8 min at 4 °C to pellet the cells. Finally, the cell concentration was adjusted to $2 \times 10^{\wedge 5}$ cells per mL using staining buffer, ready for further analysis or experimentation. Fluorescently labeled primary antibodies were added to the cell suspension and incubated in the dark at 4 °C for 30 min. The following antibodies were used: BV605-Fixable Viability Stain 575 V (BD Pharmingen), BV650-F4/80 (BioLegend, San Diego, CA), FITC-CD45 (BioLegend), APC/Cy7-NK1.1 (BioLegend), APC-CD3 (BioLegend), PE/Cy7-DX5 (BioLegend), PE-CD11C (BioLegend), BV421-Ly6G (BioLegend), BV711-CD107a (BioLegend), PE594-IFN-γ (BioLegend) and TruStain FcX™ (anti-mouse CD16/32) antibody (Biolegend). Expression of target proteins on the isolated lymphocytes was detected using a FACS Celesta™ Flow Cytometer (BD Biosciences, NJ, USA).

2.14. Statistical analysis

All experiments have at least three independent replicates. The comparison between the two groups was conducted using *t*-test or Kruskal Wallis test. Multiple groups were analyzed using one-way ANOVA or Kruskal Wallis test. Statistical analyses were performed using SPSS version 25.0 software. All data were presented in the form of mean ± standard deviation, with reported *P*-values falling below 0.05, indicating statistical significance. All graphics were created using Graphpad Prism.

3. Results

3.1. DOX induces ALI in mice

To establish a mouse model of ALI, the mice was treated with different concentrations of DOX (1 mg/kg, 5 mg/kg, 10 mg/kg, 20 mg/kg, and 40 mg/kg). The mortality rates of mice treated with DOX at concentrations of 10 mg/kg, 20 mg/kg, and 40 mg/kg exceeded 50 % on day 10. In contrast, a survival rate of mice treated with 1 mg/kg and 5 mg/kg was 100 % and 80 % respectively on day 10. Therefore, we determined that 5 mg/kg was the appropriate concentration (Fig. 1a). On the seventh day after treatment with DOX (5 mg/kg), the body weight of mice in the DOX group significantly decreased compared to the control group (Ctrl) (Fig. 1b). The serum alanine aminotransferase (ALT) and aspartate aminotransferase (AST) levels in the DOX group were significantly upregulated (Fig. 1c, d), while the glutathione (GSH) levels in liver tissue were significantly reduced (Fig. 1e). H&E staining revealed increased hepatocyte ballooning degeneration and necrosis in the DOX group (Fig. 1f), indicating that DOX induced ALI in mice.

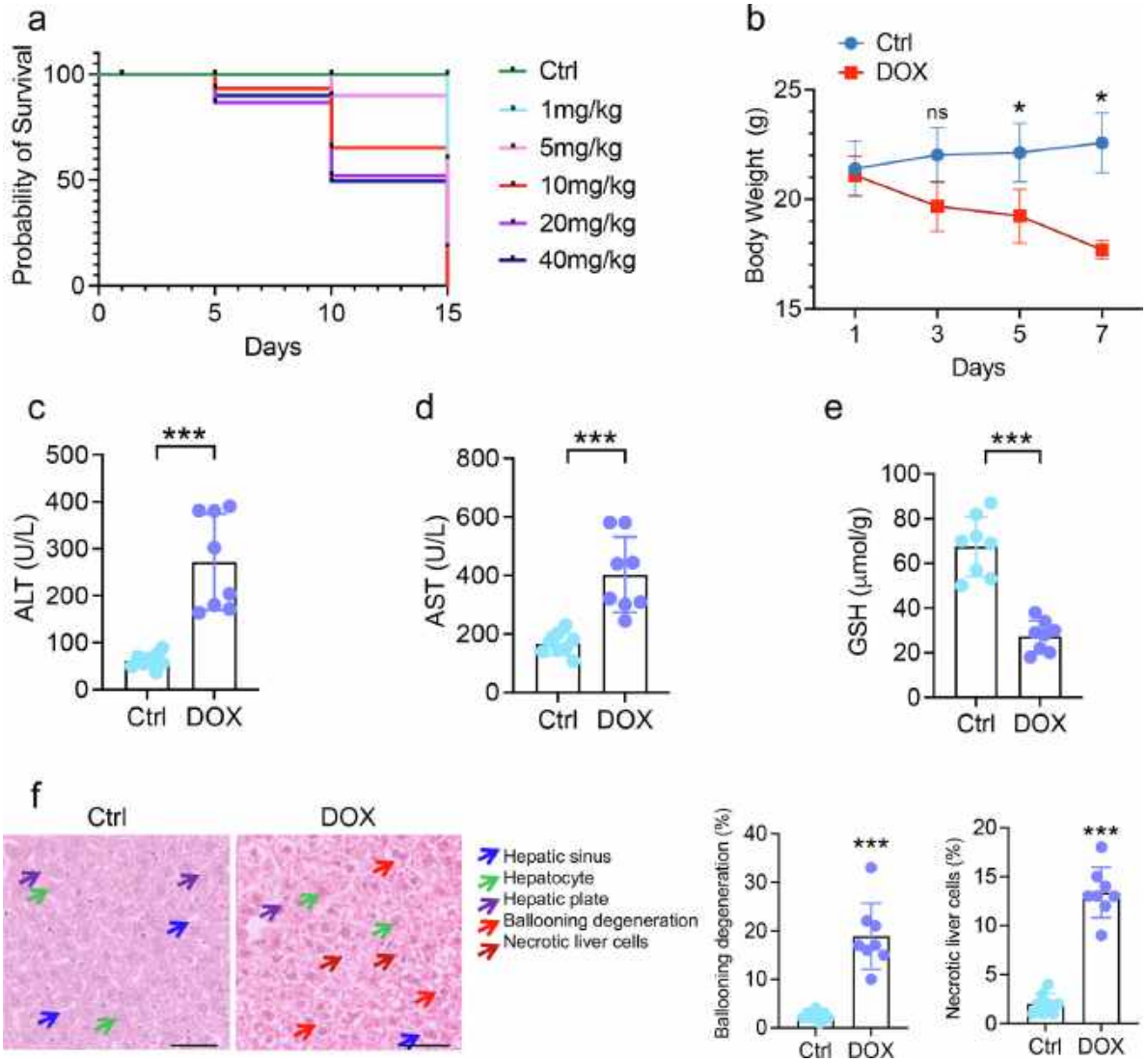

Fig. 1. DOX induces ALI in mice. (a) Survival times of mice treated with different concentrations of DOX (1 mg/kg, 5 mg/kg, 10 mg/kg, 20 mg/kg, and 40 mg/kg) were recorded. $N = 10$. (b) Changes in mouse body weight were monitored and recorded every two days. $N = 8$. Non-parametric *t*-test were used for statistical analysis. (c–e) AST, ALT, and GSH levels were measured. N = 8. Unpaired t-test was used for statistical analysis. (f) H&E staining was used to detect changes in liver tissue structure. Bar = 50 μM. The data was analyzed using unpaired *t*-tests. N = 8. $^{*}P < 0.05$; $^{***}P < 0.001$.

3.2. DOX exposure alters the metabolic profile and innate immune response signaling

To evaluate the impact of DOX on the metabolic profile and innate immune response signaling in the liver, we conducted 4D-DIA quantitative proteomics sequencing. Compared to the Ctrl group, the DOX group exhibited upregulation of 880 proteins and downregulation of 962 proteins (Fig. 2a, b). KEGG enrichment analysis of these differentially expressed proteins revealed the most significant enrichment in metabolic pathways (Fig. 2c). Among the metabolic pathways, the most notable changes were observed in tryptophan metabolism, retinol metabolism, purine metabolism, nucleotide metabolism, fatty acid metabolism, and cysteine and methionine metabolism (Fig. 2d). In terms of signal transduction pathways, the PPAR signaling pathway, PI3K-Akt signaling pathway, and NOD-like receptor signaling pathway showed the most pronounced alterations (Fig. 2e). Additionally, various cell death pathways, including ferroptosis, apoptosis, necroptosis, and autophagy, were also significantly enriched (Fig. 2f). These findings suggest that DOX exposure results in the remodeling of the hepatic proteomic metabolic profile, induction of cell damage and death, and subsequent inflammation, thereby exacerbating disruptions in liver metabolism and immune function.

3.3. DOX activates the L-tryptophan/L-kynurenine metabolic pathway

Given that DOX reshapes the metabolic profile, we subsequently employed a comprehensive targeted metabolomics approach to analyze which metabolites undergo changes. Heatmaps of metabolite clustering and volcano plots of differential metabolites illustrate the impact of DOX treatment on the metabolic profile of mouse liver tissue (Fig. 3a, b). DOX treatment upregulated 359 metabolites and downregulated 266 (Fig. 3c). KEGG enrichment and network analysis of these differential metabolites revealed significant upregulation in amino acid metabolism (Fig. 3d). Notably, L-Tryptophan (L-Try), L-lysine, and citrulline exhibited the most the most significant upregulation (Fig. 3e). To identify key regulatory points between amino acid and protein expression following DOX treatment, we utilized two-way orthogonal partial least squares (O2PLS) analysis, which revealed the closest correlation between L-Try and protein expression (Fig. 3f). Furthermore, we found that the abundance of L-kynurenine (L-Kyn), a metabolite of L-Try, was also upregulated (Fig. 3g). In particular, the expression of Indoleamine 2,3-dioxygenase 2 (IDO2), a key enzyme regulating tryptophan

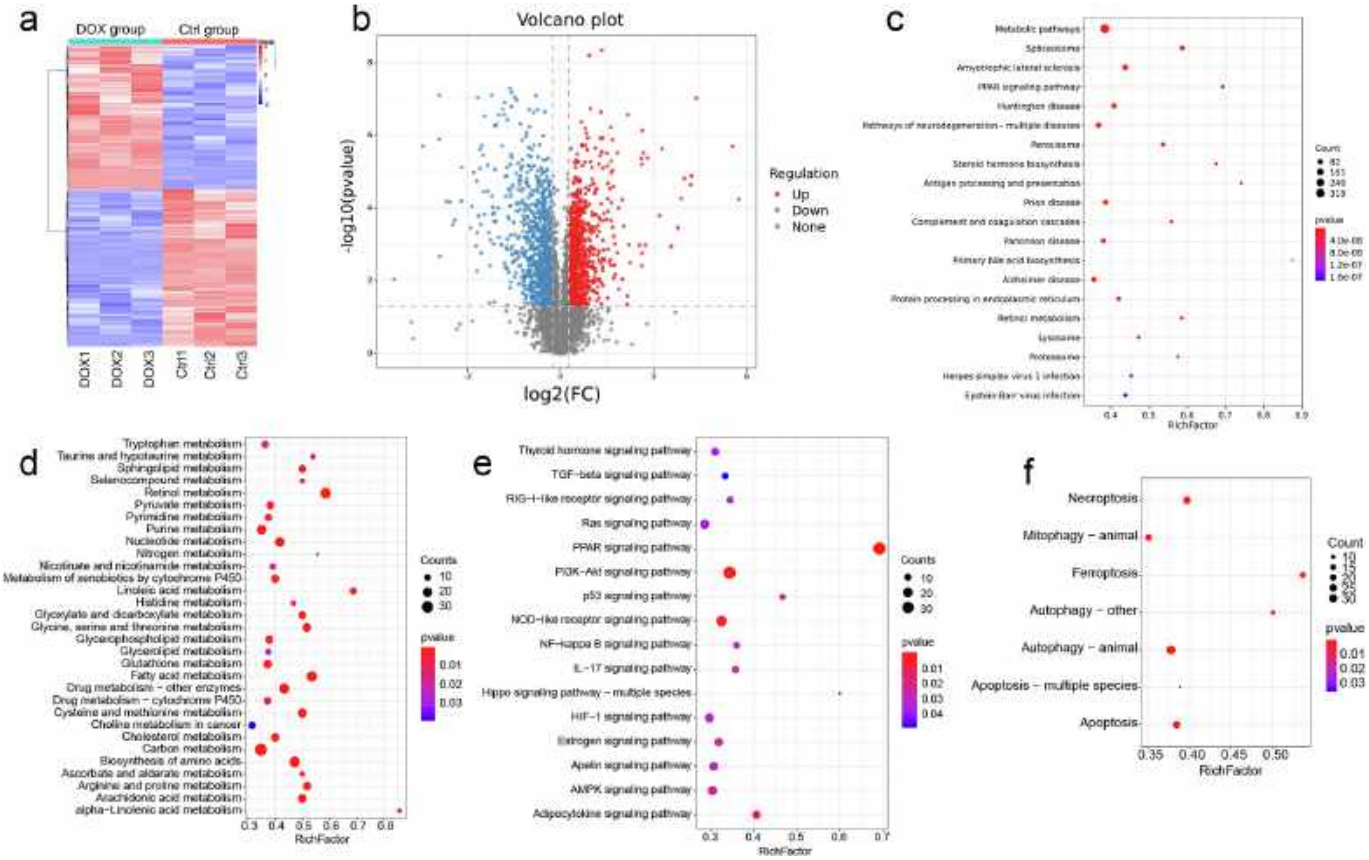

Fig. 2. DOX exposure changes the metabolic profile and innate immune response signaling in mouse liver. (a) Heatmap of clustered differentially expressed proteins. $N = 3$. (b) Volcano plot of differentially expressed proteins. Red indicates upregulated proteins, and blue indicates downregulated proteins. (c–e) Scatter plot and bubble plot of KEGG enrichment analysis. Each point in the plot represents a KEGG pathway, with colour indicating the significance of enrichment (redder colors indicate greater significance), and point size representing the number of differentially expressed proteins (larger points indicate a higher number of differentially expressed proteins). (For interpretation of the references to colour in this figure legend, the reader is referred to the web version of this article.)

metabolism, was upregulated in the DOX group (Fig. 3h). ELISA analysis also showed a significant increase in serum L-Kyn concentrations in mice treated with DOX. These data suggest that DOX activates the L-tryptophan/L-kynurenine metabolic pathway.

3.4. DOX promotes L-Kyn production through activation of IDO2

To investigate whether DOX promotes L-Kyn production through IDO2, we developed DOX-resistant hepatocyte (HepaRG/R) cells. Western blot analysis indicated a upregulation of IDO2 protein expression in HepaRG/R cells (Fig. 4a). Furthermore, mass spectrometry analysis also showed a marked elevation in L-Kyn concentrations in the supernatants of HepaRG/R cells (Fig. 4b). Subsequently, we employed short hairpin RNA (shRNA) targeting IDO2, which significantly inhibited DOX-induced L-Kyn production (Fig. 4c). Additionally, we conducted animal experiments using an IDO2 inhibitor (IDO2-IN-1) (Fig. 4d). ELISA analysis showed that the DOX-induced elevation in L-Kyn could be effectively suppressed by IDO2-IN-1 (Fig. 4e). H&E staining shows that IDO2-IN-1 can restore DOX-induced hepatocyte balling degeneration and necrosis (Fig. 4f). IDO2-IN-1 also suppressed DOX-induced ALT, AST and promote DOX-inhibited GSH (Fig. 4g). These findings indicates that DOX enhances L-Kyn production by upregulating IDO2 expression in hepatocytes.

3.5. DOX promotes NK cell dysfunction by enhancing L-Kyn production

The regulation of innate immunity plays a complex role in the progression of DILI is complex. Natural killer (NK) cells are integral to innate immune responses, participating in cell-mediated cytotoxicity and the secretion of cytotoxic granules, thereby contributing to DILI progression [18]. Previous studies have shown that L-Kyn inhibits the activity and cytotoxic capacity of NK cells [19]. Consequently, we speculated that DOX might affect the activity and cytotoxic capacity of NK cells by upregulating L-Kyn. To elucidate the mechanism of NK cells in ALI, we conducted FCM analysis, which revealed that DOX treatment inhibited NK cell infiltration and reduced the expression levels of CD107a and IFN-γ in NK cells within mouse liver tissue (Fig. 5a). This suggests that DOX diminishes the degranulation ability and cytotoxic capacity of NK cells. Further FCM analysis revealed that treatment with IDO2-IN-1 could restore NK cell infiltration and increase the expression of CD107a and IFN-γ in NK cells (Fig. 5b). Additionally, ELISA analysis demonstrated that DOX induced the secretion of TNF-α, IL-1β, and IL-6, while inhibiting the secretion of IL-10, and these effects could be reversed by treatment with IDO2-IN-1 (Fig. 5c). These findings propose that DOX-induced L-Kyn inhibits the activity and cytotoxic capacity of NK cells.

3.6. Targeting the Kyn-AhR axis reverse DOX-induced ALI

The primary receptor for L-Kyn is the aryl hydrocarbon receptor (AhR) [20]. To clarify whether DOX-induced NK cell dysfunction occurs *via* AhR activation, we established a coculture system where NK-92 cells pretreated with an AhR inhibitor (CH-223191, CH) were stimulated with HepaRG/S or HepaRG/R cell culture medium. qRT-PCR results showed that HepaRG/R cell culture medium promoted AhR expression in NK-92 cells while inhibiting the expression of CD107a and IFN-γ

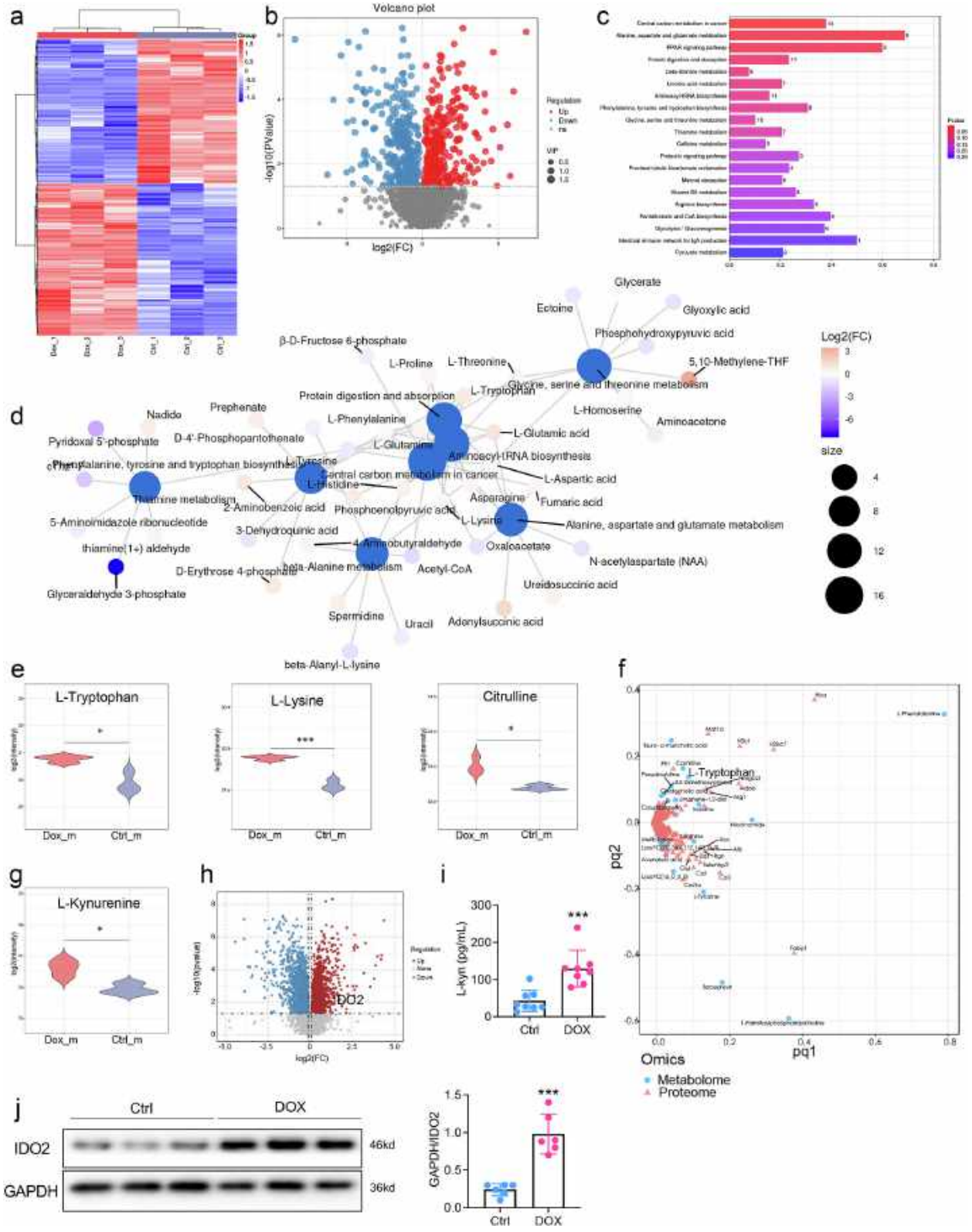

Fig. 3. DOX enhances L-Tryptophan/L-Kynurenine metabolism in mouse liver tissue. (a) Heatmap of clustered differential metabolites. N = 3. (b) Volcano plot of differential metabolites. Red indicates upregulated metabolites, and blue indicates downregulated metabolites. (c) Bar plot of metabolic pathway impact factors. (d) Network diagram. (e) Violin plots showing the abundance differences of L-Try, L-lysine, and citrulline between the Ctrl and DOX groups. N = 3. Unpaired *t*-test was used for statistical analysis. (f) O2PLS analysis. (g) Violin plot showing the abundance of L-Kyn. N = 3. Unpaired t-test was used for statistical analysis. (h) Volcano plot displaying differential proteins in the DOX group compared to the Ctrl group. (i) ELISA analysis of mouse serum L-Kyn concentrations. N = 8. The data were analyzed using unpaired t-test. (j) Western blot detection of IDO2 protein expression levels in the Ctrl and DOX groups. The data was analyzed using unpaired t-test. $N = 6$. $^{***}P < 0.001$. (For interpretation of the references to colour in this figure legend, the reader is referred to the web version of this article.)

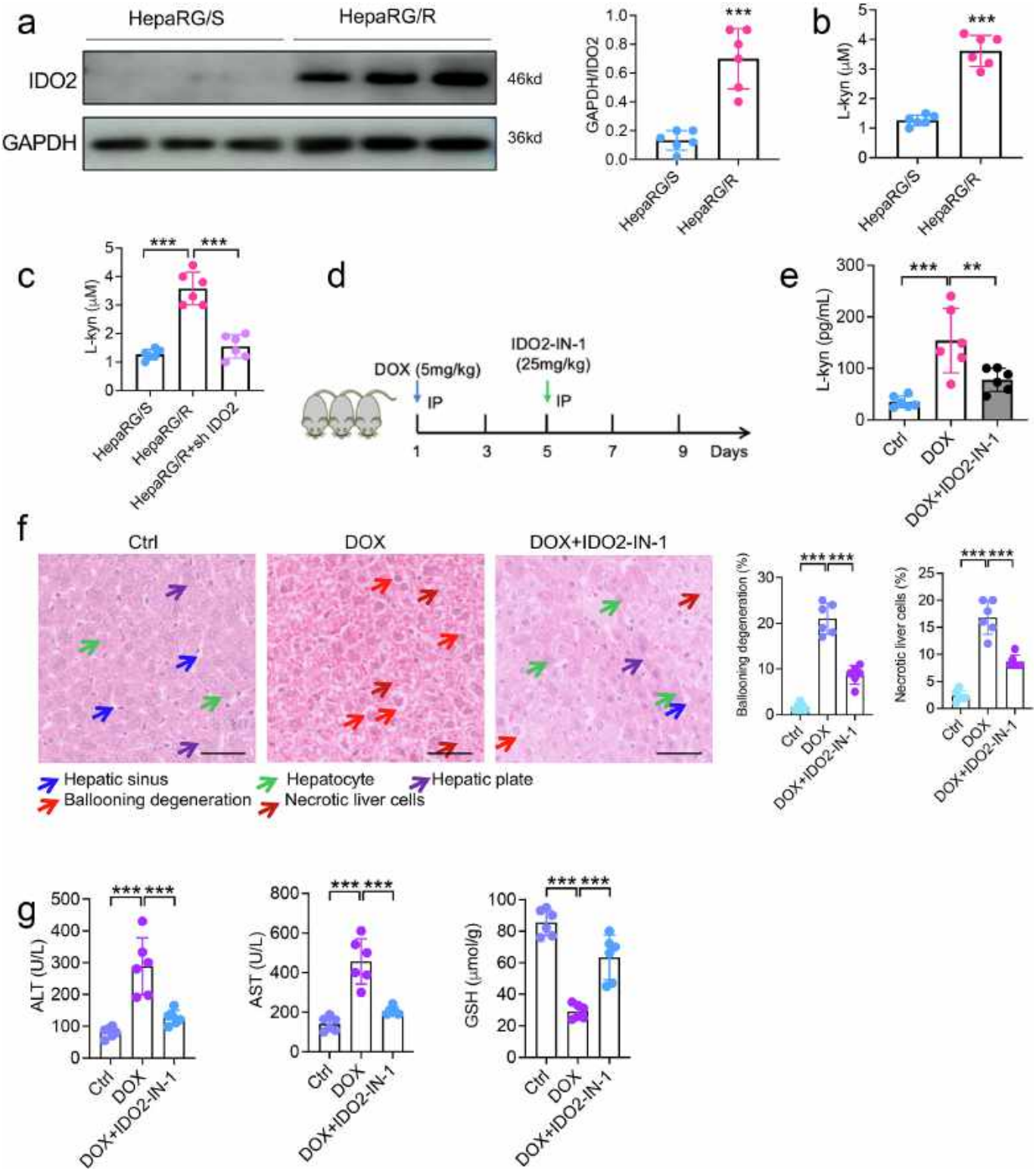

Fig. 4. DOX promotes L-Kyn production. (a) Western blot analysis of IDO2 protein expression levels in HepaRG/R and HepaRG/S cells. N = 6. The data was analyzed using unpaired t-test. (b) Mass spectrometry analysis of L-Kyn levels in the supernatants of HepaRG/R and HepaRG/S cell cultures. N = 6. The data were analyzed using unpaired t-test. (c) Mass spectrometry analysis of the effect of IDO2/shRNA on L-Kyn levels in cell culture supernatants. N = 6. The data was analyzed using one-way ANOVA. (d) Schematic diagram of the animal model with IDO2-IN-1 intervention. (e) ELISA detection of mouse serum L-Kyn concentrations. N = 6. The data was analyzed using one-way ANOVA. (f) H&E staining was used to detect changes in liver tissue structure. Bar = 50 μM. N = 6. The data was analyzed using one-way ANOVA. (g) AST, ALT, and GSH levels were measured. N = 6. The data was analyzed using one-way ANOVA. $^{**}P < 0.01$; $^{***}P < 0.001$.

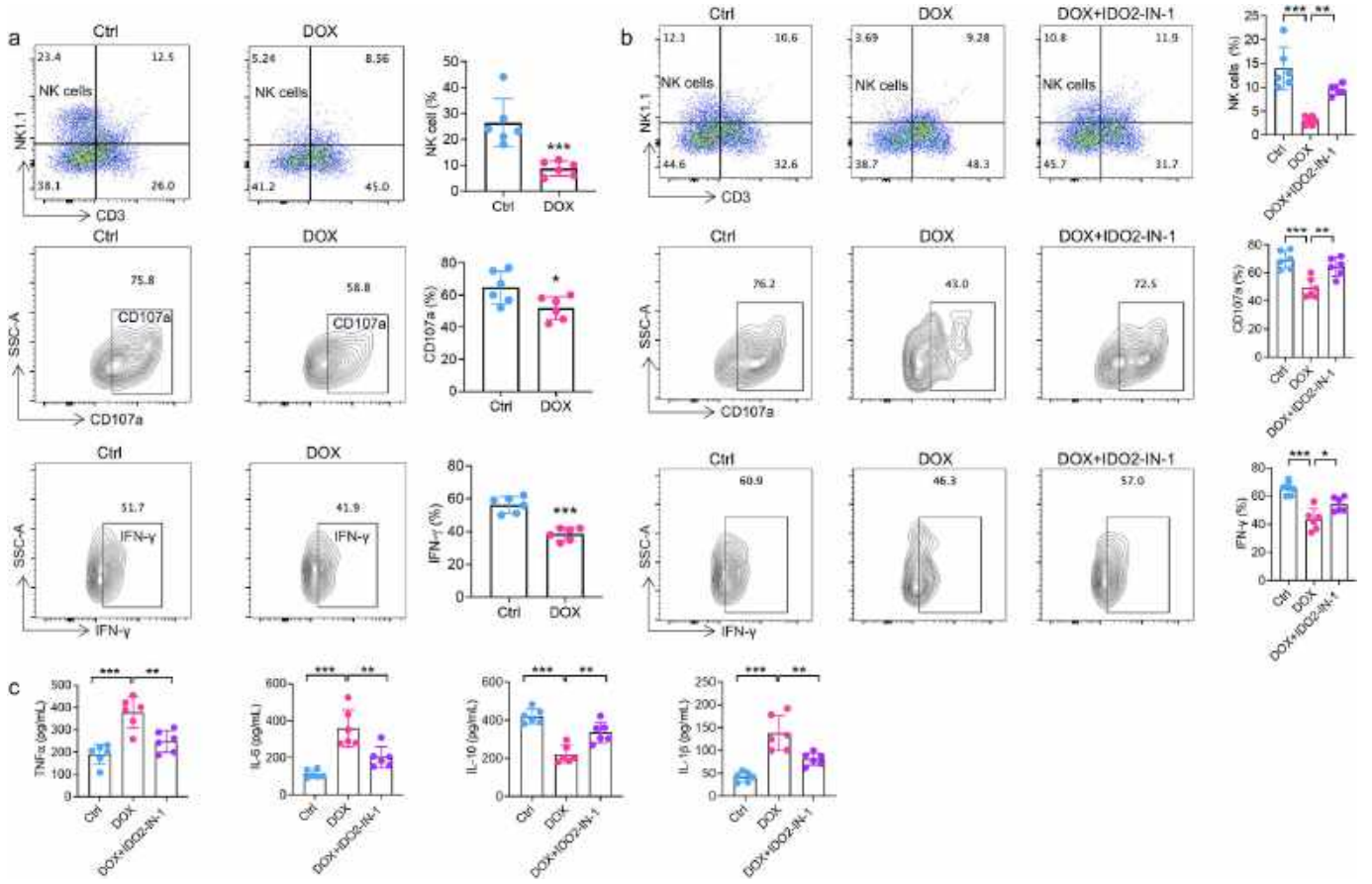

Fig. 5. DOX promotes NK cell dysfunction by enhancing L-Kyn production. (a-b) FCM analysis of NK cells and the expression levels of CD107a and IFN-γ in NK cells in mouse liver tissue. N = 6. The comparison between the two groups was conducted using unpaired t-test. The comparison between the three groups was conducted using one-way ANOVA. (c) ELISA analysis of TNF-α, IL-1β, IL-6, and IL-10 concentrations in mouse serum. N = 6. The data was analyzed using one-way ANOVA. $^{*}P < 0.05$; $^{**}P < 0.01$; $^{***}P < 0.001$.

(Fig. 6a). CH not only inhibited AhR induction by HepaRG/R cell culture medium but also restored the expression of CD107a and IFN-γ (Fig. 6a). H&E staining shows that CH can restore DOX-induced hepatocyte balling degeneration and necrosis (Fig. 6b). CH also suppressed DOX-induced ALT, AST and promote DOX-inhibited GSH (Fig. 6c). FCM analysis revealed that treatment with CH could restore NK cell infiltration (Fig. 6d). Additionally, ELISA analysis demonstrated that DOX induced the secretion of TNF-α, IL-1β, and IL-6, while inhibiting the secretion of IL-10, and these effects could also be reversed by treatment with CH (Fig. 6e). These findings suggests that DOX inhibits the expression of CD107a and IFN-γ by promoting hepatocyte secretion of L-Kyn to activate the Kyn-AhR axis. Targeting the Kyn-AhR axis can significantly improve DOX-induced ALI.

4. Discussion

As a clinically significant issue, the research on the pathogenesis of DILI is particularly important, especially for injuries caused by commonly used drugs like doxorubicin. In this study, we constructed a mouse model and employed various omics technologies to deeply explore the metabolic and immune mechanisms of DOX-induced ALI. Our findings revealed that DOX (5 mg/kg) not only altered the hepatic metabolic profile but also impacted the innate immune response, particularly by activating the IDO2-mediated metabolic pathway and the Kyn-AhR axis, leading to impaired NK cell function. These discoveries provide new insights into the treatment of DILI, and targeting the Kyn-AhR axis may emerge as an effective strategy for reversing acute liver injury in the future, warranting further research and exploration.

The changes in innate immune cells and inflammatory cytokines in mouse liver tissue exhibit a complex and specific pattern during DILI. Our previous studies showed that APAP treatment significantly increased neutrophil infiltration while inhibiting Kupffer cell infiltration, accompanied by elevated secretion of pro-inflammatory cytokines TNF-α and IL-6, and decreased secretion of the anti-inflammatory cytokine IL-10 [8]. Research suggested that the combined use of DOX and Cucurbitacin IIa (CUIIa) significantly reduced myoid derived suppressor cells, T regulatory cells and M2-polarized macrophages [21]. Our study further identifies that DOX, as another common drug inducing liver injury, operates through a different mechanism compared to APAP. DOX inhibits NK cell infiltration and induces the secretion of pro-inflammatory cytokines such as TNF-α, IL-1β, and IL-6, while suppressing the secretion of the anti-inflammatory cytokine IL-10. This imbalance in the secretion of pro-inflammatory and anti-inflammatory cytokines is likely a crucial mechanism by which DOX causes ALI. Notably, this study also unveils the significant role of tryptophan metabolism in DOX-induced liver injury. Tryptophan is metabolized into Kyn by indoleamine 2,3-dioxygenase (IDO) or tryptophan 2,3-dioxygenase (TDO) [22]. AhR, as a sensor for tryptophan metabolites, plays a pivotal role in immune regulation [23]. The Kyn produced by cells affects various immune cells by binding to AhR [24]. Some studies found that L-Kyn can induced ferroptosis in NK cells, thereby inhibiting NK cell accumulation independently of the Kyn-AhR signal [25]. However, this study indicates that DOX activates the Kyn-AhR axis, which subsequently inhibits the accumulation and activity of NK cells. Notably, this effect can be mitigated by the administration of IDO2-IN-1, implying that DOX impacts NK cell function through the activation of the Kyn-

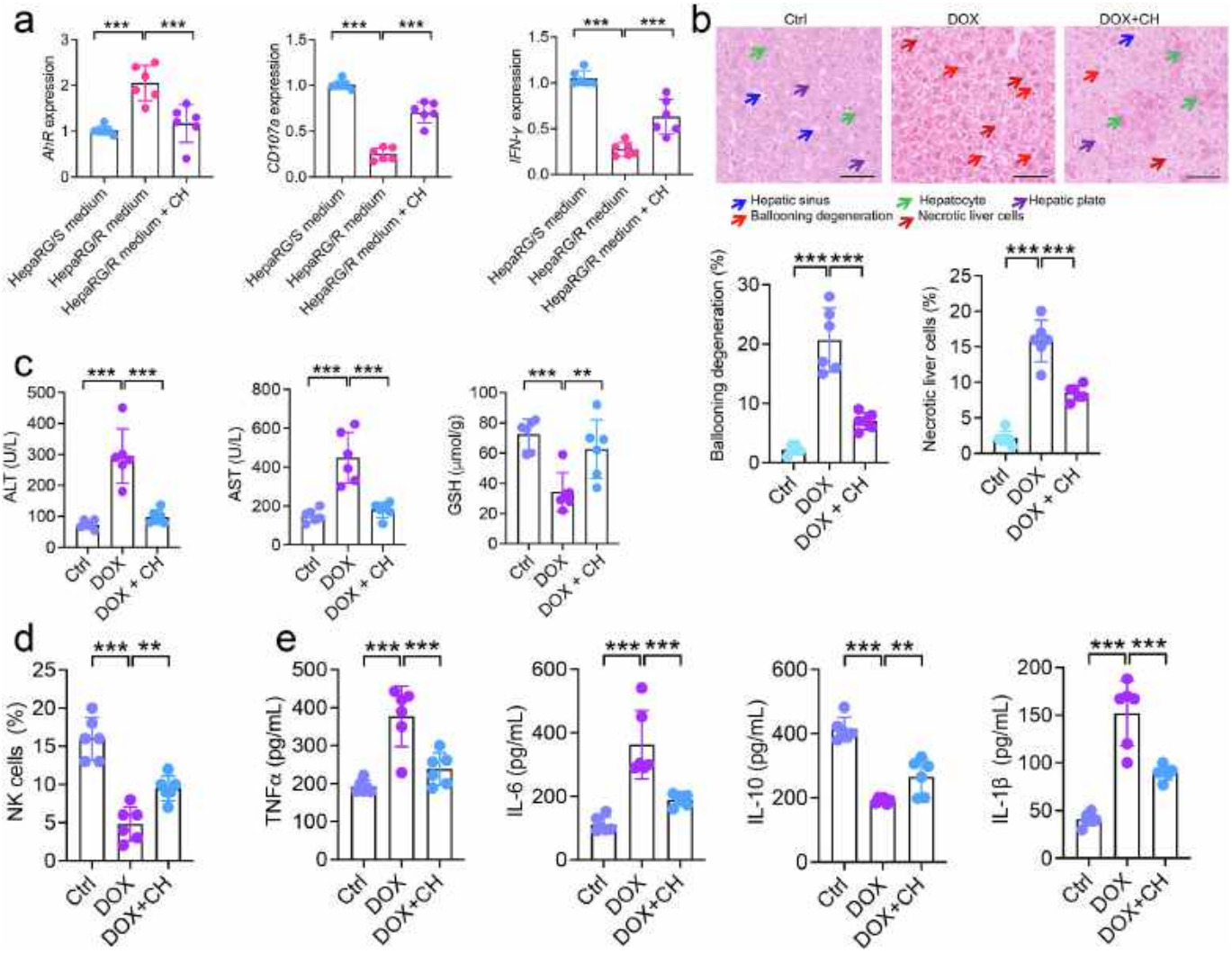

Fig. 6. Targeting the Kyn-AhR axis reverses DOX-induced ALI. (a) qRT-PCR was used to detect the mRNA expression levels of AhR, CD107a, and IFN-γ in NK-92 cells. "DOX + CH"represents the use of CH treatment on the basis of DOX treatment group. N = 6. The data was analyzed using one-way ANOVA. (b) H&E staining was used to detect changes in liver tissue structure. Bar = 50 μM. N = 6. The data was analyzed using one-way ANOVA. (c) AST, ALT, and GSH levels were measured. N = 6. The data was analyzed using one-way ANOVA. (d) FCM analysis of NK cells. N = 6. The data was analyzed using one-way ANOVA. (e) ELISA analysis of TNF-α, IL-1β, IL-6, and IL-10 concentrations in mouse serum. N = 6. The data was analyzed using one-way ANOVA. $^{**}P < 0.01$; $^{***}P < 0.001$.

AhR axis, thereby exacerbating liver injury.

Despite some progress in mitigating the side effects of DILI, patients remain at significant risk of DOX-induced hepatic toxicity. As a primary detoxifying organ, the liver is particularly vulnerable to oxidative stress. The quinone moiety of DOX can precipitate severe oxidative stress in hepatic active substances, culminating in hepatocyte necrosis. The adverse side effects associated with chemotherapy lead some patients to be hesitant about undergoing treatment. Consequently, the development of novel strategies to reduce these side effects and enhance patients' quality of life is of paramount importance. Researchers have developed compound 4t [26] and compound 22 [17] targeting IDO2, which have shown significant efficacy in treating mouse tumors or arthritis models, potentially benefiting patients receiving DOX chemotherapy. A randomized double-blind controlled study conducted in China assessed the efficacy and safety of magnesium isoglycyrrhizinate, a hepatoprotective agent, in the treatment of DILI. The study demonstrated that both low-dose and high-dose regimens significantly ameliorated liver injury compared to the control group, leading to the approval of the drug for the treatment of acute DILI. Another promising drug for DILI treatment, bicyclol, has passed Phase II clinical studies. Additionally, recent research has found that astaxanthin improves DOX-induced liver injury in mice through the Keap1/Nrf2/HO1 pathway [27]. Despite conducting an in-depth exploration of the metabolic and immune mechanisms of DOX-induced ALI in mouse models using multi-omics techniques, and revealing the pivotal role of the Kyn-AhR axis in impairing NK cell function and exacerbating liver injury, thereby providing a new perspective for the treatment of DILI, this study still has some limitations. For example, this research primarily focuses on mouse models, whereas the pathogenesis of human DILI may be more complex, involving numerous genetic, environmental, and individual factors. Furthermore, although our study suggests that targeting the Kyn-AhR axis may be a promising therapeutic strategy, further preclinical and clinical studies are required to verify its safety and efficacy.

5. Conclusions

Our study reveals DOX-induced ALI mechanisms involving metabolic and immune alterations, particularly Kyn-AhR axis activation impairing NK cells. Targeting this pathway offers a promising strategy for DILI treatment.

Data and materials will be made available on request.

CRediT authorship contribution statement

Bohuai Tang: Writing – original draft, Formal analysis, Data curation, Conceptualization. **Huan Ouyang:** Conceptualization, Data curation, Formal analysis, Writing – original draft. **Shuping Zheng:** Writing – original draft, Formal analysis, Data curation, Conceptualization. **Le Yu:** Visualization, Validation, Software, Methodology, Investigation. **Ruiying Xiao:** Visualization, Validation, Software, Methodology, Investigation. **Linqing Wu:** Writing – review & editing, Project administration, Funding acquisition, Conceptualization. **Zengbin Wang:** Writing – review & editing, Supervision, Funding acquisition, Conceptualization.

Declaration of competing interest

The authors declare that they have no known competing financial interests or personal relationships that could have appeared to influence the work reported in this paper.

Acknowledgements

This work was supported by the the Scientific Research Project of Fujian Education Department (JZ230018), the Fujian Provincial Natural Science Foundation of China (2024J08052), the National Natural Science Foundation of China (82403155) and the startup grant for High-level Talents of Fujian Medical University (XRCZX2023024). The authors thank the Public Technology Service Center Fujian Medical University for their help and technical support.

Data availability

Data and materials will be made available on request.

References

[1] T. Shen, Y. Liu, J. Shang, Q. Xie, J. Li, M. Yan, J. Xu, J. Niu, J. Liu, P.B. Watkins, G. P. Aithal, R.J. Andrade, X. Dou, L. Yao, F. Lv, Q. Wang, Y. Li, X. Zhou, Y. Zhang, P. Zong, B. Wan, Z. Zou, D. Yang, Y. Nie, D. Li, Y. Wang, X. Han, H. Zhuang, Y. Mao, C. Chen, Incidence and etiology of drug-induced liver injury in mainland China, Gastroenterology 156 (8) (2019) 2230–2241.e11.

[2] C. Liu, C. Zhang, T. He, L. Sun, Q. Wang, S. Han, W. Wang, J. Kong, F. Yuan, J. Huang, Study on potential toxic material base and mechanisms of hepatotoxicity induced by Dysosma versipellis based on toxicological evidence chain (TEC) concept, Ecotoxicol. Environ. Saf. 190 (2020) 110073.

[3] A.T. Al Khafaji, A.M. Barakat, A.J. Shayyal, A.A. Taan, R.F. Aboqader Al-Aouadi, Managing doxorubicin cardiotoxicity: insights into molecular mechanisms and protective strategies, J. Biochem. Mol. Toxicol. 39 (2) (2025) e70155.

[4] H. Zhang, S. Xie, W. Deng, Mitophagy in doxorubicin-induced cardiotoxicity: insights into molecular biology and novel therapeutic strategies, Biomolecules 14 (12) (2024).

[5] S. Gao, W. Wang, J. Li, Y. Wang, Y. Shan, H. Tan, Unveiling polysaccharides of Houttuynia cordata Thunb.: extraction, purification, structure, bioactivities, and structure-activity relationships, Phytomedicine 138 (2025) 156436.

[6] S. Gao, J. Li, W. Wang, Y. Wang, Y. Shan, H. Tan, Rabdosia rubescens (Hemsl.) H., Hara: a potent anti-tumor herbal remedy - botany, phytochemistry, and clinical applications and insights, J. Ethnopharmacol. 340 (2025) 119200.

[7] S. Gao, Y. Shan, Y. Wang, W. Wang, J. Li, H. Tan, Polysaccharides from Lonicera japonica Thunb.: extraction, purification, structural features and biological activities-a review, Int. J. Biol. Macromol. 281 (Pt 4) (2024) 136472.

[8] Z. Wang, L. Wu, B. Pan, Y. Chen, T. Zhang, N. Tang, Interleukin 33 mediates hepatocyte autophagy and innate immune response in the early phase of acetaminophen-induced acute liver injury, Toxicology 456 (2021) 152788.

[9] F. Yarmohammadi, R. Rezaee, G. Karimi, Natural compounds against doxorubicin-induced cardiotoxicity: a review on the involvement of Nrf2/ARE signaling pathway, Phytother. Res. 35 (3) (2021) 1163–1175.

[10] T. Afsar, S. Razak, A. Almajwal, Effect of Acacia hydaspica R, Parker extract on lipid peroxidation, antioxidant status, liver function test and histopathology in doxorubicin treated rats, Lipids Health Dis. 18 (1) (2019) 126.

[11] F. Yarmohmmadi, N. Rahimi, H. Faghir-Ghanesefat, N. Javadian, A. Abdollahi, P. Pasalar, F. Jazayeri, S. Ejtemaeemehr, A.R. Dehpour, Protective effects of agmatine on doxorubicin-induced chronic cardiotoxicity in rat, Eur. J. Pharmacol. 796 (2017) 39–44.

[12] M. Sheibani, S. Nezamoleslami, H. Faghir-Ghanesefat, A.H. Emami, A.R. Dehpour, Cardioprotective effects of dapsone against doxorubicin-induced cardiotoxicity in rats, Cancer Chemother. Pharmacol. 85 (3) (2020) 563–571.

[13] J.J. Guo, L.L. Ma, H.T. Shi, J.B. Zhu, J. Wu, Z.W. Ding, Y. An, Y.Z. Zou, J.B. Ge, Alginate oligosaccharide prevents acute doxorubicin cardiotoxicity by suppressing oxidative stress and endoplasmic reticulum-mediated apoptosis, Mar. Drugs 14 (12) (2016).

[14] K.P. Hopfner, V. Hornung, Molecular mechanisms and cellular functions of cGAS-STING signalling, Nat. Rev. Mol. Cell Biol. 21 (9) (2020) 501–521.

[15] Z. Wang, P. Sun, B. Pan, J. Qiu, X. Zhang, S. Shen, X. Ke, N. Tang, IL-33/ST2 antagonizes STING signal transduction via autophagy in response to acetaminophen-mediated toxicological immunity, Cell Commun. Signal. 21 (1) (2023) 80.

[16] A. El-Zawahry, J. McKillop, C. Voelkel-Johnson, Doxorubicin increases the effectiveness of Apo2L/TRAIL for tumor growth inhibition of prostate cancer xenografts, BMC Cancer 5 (2005) 2.

[17] G. He, S. Wan, Y. Wu, Z. Chu, H. Shen, S. Zhang, L. Chen, Z. Bao, S. Gu, J. Huang, L. Huang, G. Gong, Y. Zou, Q. Zhu, Y. Xu, Discovery of the first selective IDO2 inhibitor as novel immunotherapeutic avenues for rheumatoid arthritis, J. Med. Chem. 65 (21) (2022) 14348–14365.

[18] Y. Qian, J. Zhao, H. Wu, X. Kong, Innate immune regulation in inflammation resolution and liver regeneration in drug-induced liver injury, Arch. Toxicol. (2024).

[19] M. Della Chiesa, S. Carlomagno, G. Frumento, M. Balsamo, C. Cantoni, R. Conte, L. Moretta, A. Moretta, M. Vitale, The tryptophan catabolite L-kynurenine inhibits the surface expression of NKp46- and NKG2D-activating receptors and regulates NK-cell function, Blood 108 (13) (2006) 4118–4125.

[20] J.E. Cheong, L. Sun, Targeting the IDO1/TDO2-KYN-AhR pathway for Cancer immunotherapy - challenges and opportunities, Trends Pharmacol. Sci. 39 (3) (2018) 307–325.

[21] S. Li, S. Wang, A. Zhang, L. Luo, J. Song, G. Wei, Z. Fang, Cucurbitacin IIa promotes the immunogenic cell death-inducing effect of doxorubicin and modulates immune microenvironment in liver cancer, Int. J. Oncol. 64 (4) (2024).

[22] I. Cervenka, L.Z. Agudelo, J.L. Ruas, Kynurenines: Tryptophan's metabolites in exercise, inflammation, and mental health, Science (New York, N.Y.) 357 (6349) (2017).

[23] K. Minton, Negative regulation of AHR essential for intestinal homeostasis, Nat. Rev. Immunol. 23 (4) (2023) 202.

[24] E.F. de Araújo, F.V. Loures, N.W. Preite, C. Feriotti, N.A. Galdino, T.A. Costa, V.L. G. Calich, AhR ligands modulate the differentiation of innate lymphoid cells and T helper cell subsets that control the severity of a pulmonary fungal infection, Front. Immunol. 12 (2021) 630938.

[25] J.X. Cui, X.H. Xu, T. He, J.J. Liu, T.Y. Xie, W. Tian, J.Y. Liu, L-kynurenine induces NK cell loss in gastric cancer microenvironment via promoting ferroptosis, J. Exp. Clin. Cancer Res. 42 (1) (2023) 52.

[26] X. He, G. He, Z. Chu, H. Wu, J. Wang, Y. Ge, H. Shen, S. Zhang, J. Shan, K. Peng, Z. Wei, Y. Zou, Y. Xu, Q. Zhu, Discovery of the first potent IDO1/IDO2 dual inhibitors: a promising strategy for Cancer immunotherapy, J. Med. Chem. 64 (24) (2021) 17950–17968.

[27] H. Ma, S. Chen, H. Xiong, M. Wang, W. Hang, X. Zhu, Y. Zheng, B. Ge, R. Li, H. Cui, Astaxanthin from Haematococcus pluvialis ameliorates the chemotherapeutic drug (doxorubicin) induced liver injury through the Keap1/Nrf2/HO-1 pathway in mice, Food Funct. 11 (5) (2020) 4659–4671.